# Defect pinning of interface motion in thermoelastic structural transitions of Cu-Al-Ni shape-memory alloy

J. I. Pérez-Landazábal,[1,*] V. Recarte,[1] D. S. Agosta,[2] V. Sánchez-Alarcos,[1] and R. G. Leisure[2]
[1]*Departamento de Física, Universidad Pública de Navarra, Campus de Arrosadía, 31006 Pamplona, Spain*
[2]*Department of Physics, Colorado State University, Fort Collins, Colorado 80523-1875, USA*
(Received 17 January 2006; revised manuscript received 14 March 2006; published 1 June 2006)

The high mobility of austenite-martensite interfaces is a characteristic of a thermoelastic martensitic transformation. Internal friction and elastic constants are very suitable probes to analyze this mobility. In this work, resonant ultrasound spectroscopy, differential scanning calorimetry, and neutron powder diffraction have been employed to analyze the role of defects in a first-order transformation. An anomalous behavior associated with the martensitic transformation in a Cu-Al-Ni shape-memory alloy has been observed; the internal friction peak measured during cooling completely disappears on heating. The elastic constants also show different behavior on heating and cooling. The different mobility of defects in the two phases, and the simultaneous occurrence of both the defect recovery processes and the martensitic transformation in the same temperature range, are the origin of the observed behavior. These effects show an exceptional influence of defects on thermoelastic equilibrium during a first-order structural transition. The proposed mechanism is general and may apply to other transitions than the one reported in this paper.

DOI: 10.1103/PhysRevB.73.224101 PACS number(s): 81.30.Kf, 62.40.+i, 81.40.−z, 61.82.Bg

## I. INTRODUCTION

The martensitic transformation (MT) is a first-order diffusionless phase transition from a symmetric high-temperature bcc phase (austenite or $\beta$ phase) to a low-symmetry, close-packed phase (martensite) that appears during cooling,[1] where the resultant lattice distortion can be essentially described by shears.[2] This kind of transition has been the subject of extensive research due to the shape-memory effect and the magnetostrictive properties associated with the MT, shown by shape-memory alloys (SMA).[2] In Cu-based SMA the $\beta$ phase is stabilized by an excess of vibrational entropy compared with the martensitic structure.[3] This excess entropy, related to the low-energy thermoacoustic $TA_2$ [110] phonon branch with its correspondingly small value of the $C'$ elastic constant, is responsible for the lattice instability of the $\beta$ phase at low temperatures.[4] In addition, on cooling $C'$ softens when the MT is approached,[5–8] and the restoring forces diminish in specific lattice directions of the $\beta$ phase. The transformation proceeds as a combination of shears and shuffles on {110} planes along $\langle 1\bar{1}0\rangle$ directions.[4]

During a first-order transformation both phases are present and austenite-martensite interfaces appear. A characteristic of a thermoelastic MT is the high mobility of these interfaces.[9] The dynamic behavior of the interfaces has been analyzed within the framework of lattice dislocation dynamics.[10] In a thermoelastic MT, the deformation produced by the lattice shearing is stored as elastic energy.[9] Thus, in the transformation region there is a local equilibrium between the difference in chemical Gibbs free energy (between $\beta$ and martensite phases), the stored elastic energy, and the energy dissipated by the frictional forces.[11] The balance between the different energy terms[12,13] (neglecting external fields) can be modified by internal stresses, degree of order, precipitation of stable phases, defects, composition, etc. All these parameters influence and determine the characteristics of the MT.

Much attention must be given to the microstructural state of the high-temperature $\beta$ phase near the phase transformation in order to analyze the role of defects in the martensite nucleation process,[14] and in the mobility of interfaces.[10,15] On the other side, the low-temperature phase and, in particular, the stabilization of the martensite (an increase in the temperature of the first reverse transformation to the parent phase) have been the subject of several studies. This stabilization has been explained by changes in the degree of long-range order, modification of the short-range order configuration of the lattice imperfections, pinning of martensite variant domains, or changes in the nature of the fault structure of the martensite.[16] Regarding the mechanical pinning of interfaces by quenched-in defects, two mechanisms have been proposed: a static pinning due to isothermal aging in martensite state[17] and a kinetic pinning of interfaces during the first reverse transformation linked to the sweeping up of quenched-in defects by moving interfaces.[18]

The aim of the present paper is to experimentally study the effect of defects on a first-order transformation through the analysis of the influence of quenched defects on the dynamics of the transformation, and on the local thermoelastic equilibrium of $\beta$-martensite interfaces during the MT in Cu-Al-Ni SMA. For this purpose, an alloy undergoing the MT in the same temperature range where the annealing of defects takes place has been chosen. In addition to the experimental observation of this effect, the pinning of interface movements by quenched-in defects has been proposed as the physical mechanism to explain the absence of the peak during the reverse transformation. The results show the crucial role of defects on thermoelastic equilibrium during a first-order phase transition. The proposed mechanism is general, and may apply to other transitions than the one reported in this paper. The paper is organized as follows: in Sec. II the experimental methods are described. The experimental results are presented in Sec. III. In Sec. IV we discuss the results obtained and, finally, conclusions are outlined in Sec. V.

 

## II. EXPERIMENT

Polycrystalline samples of a $Cu_{71}Al_{26}Ni_3$ SMA processed by powder metallurgy and hot isostatic pressing (HIP) have been used. This processing technique avoids preferential grain orientation (texture).[19,20] The samples were annealed at 1173 K during 1.8 ks and quenched in ice water. To characterize the MT, three experimental techniques have been used: neutron diffraction (ND), differential scanning calorimetry (DSC), and resonant ultrasound spectroscopy (RUS).

The characteristic MT temperatures and enthalpies have been determined by a (TA) Q100 differential scanning calorimeter (DSC). Cooling-heating DSC cycles at 10 K $min^{-1}$ were performed in order to measure the forward ($\beta \rightarrow$ martensite) and reverse (martensite $\rightarrow \beta$) MTs. Intermediate thermal treatments were also performed at the same heating rate up to different temperatures. After removing the baseline, the transformation enthalpy, $\Delta H$, was estimated using the following expression:

$$\Delta H = \int_{start}^{end} \frac{dQ}{dt} \left| \frac{dT}{dt} \right|^{-1} dT, \tag{1}$$

where $Q$ is the heat exchanged between the sample and surroundings and $dT/dt$ is the heating-cooling rate.

Powder ND studies were performed at the D20 and D1A installations at the Institut Laue-Langevin. The neutron wavelengths were $\lambda = 1.3$ Å and $\lambda = 1.9114$ Å, respectively. To study the MT, samples were cycled at 10 K $min^{-1}$ through the transformation and each spectrum was measured during 1 min. High-resolution measurements at room temperature were made at the D1A installation to determine the structure of the martensitic phase.

Measurements of elastic constants and internal friction by RUS of the as-quenched samples on heating and cooling through the MT have been performed using a small sample holder in a cryostat, and placing a thermocouple near the sample. RUS can be used to characterize the elastic properties of a wide range of solid-state materials by measuring their resonance spectra.[21,22] The elastic constants are determined after fitting the experimental resonance frequencies of the sample with theoretical resonances predicted from the sample shape, mass, and preliminary elastic constants. A DRS Inc. Modulus II system has been used to analyze the resonant ultrasonic spectrum. A rectangular parallelepiped of $1.6032 \times 1.3818 \times 2.5466$ $mm^3$ and mass = 0.04040 g was used for the RUS technique. To fit the experimental spectrum to the theoretical one, precision of 1 $\mu$m/mm is required for parallelism and perpendicularity between the faces of the parallelepiped. The lack of preferential grain orientation allows one to consider the material as isotropic, and consequently its elastic behavior defined by $C_{11}$ and $C_{44}$. The frequencies of the lowest 23 resonances were measured with a typical rms difference between measured and computed frequencies of 0.2% or less. Typical scans run from 300 to 1300 kHz. In general a given RUS eigenmode may depend on several elastic constants and the eigenfrequencies $f_n = f_n(C_{11}, C_{44})$ have different sensitivities to $C_{ij}$. RUS internal friction (IF) values were determined from the width of the resonance peak.

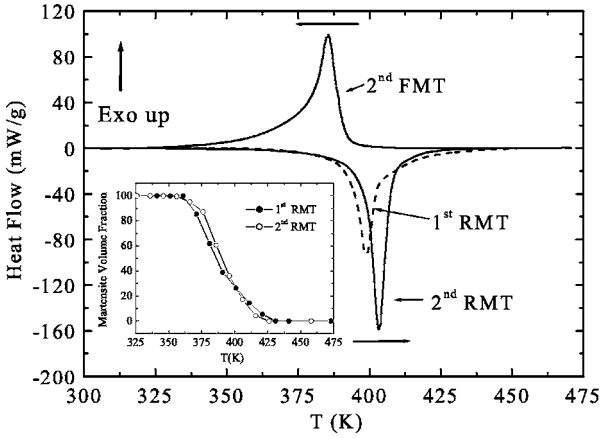


FIG. 1. DSC thermogram corresponding to the first reverse MT (1st RMT) in the as-quenched state (dashed line) and the second forward MT (2nd FMT) and second reverse MT (2nd RMT) (full line). The inset shows the martensite volume fraction determined by neutron diffraction during the first RMT (as-quenched) and during the second RMT.

## III. RESULTS

Figure 1 shows the DSC thermogram measured during heating corresponding to the as-quenched sample (dashed line). The first reverse MT (labeled 1st RMT on the figure) appears as an endothermic peak at around 400 K. After heating to 473 K, the forward and reverse MT, second forward MT (labeled FMT), and second reverse MT (labeled 2nd RMT), respectively, were measured during cooling and heating (full line in Fig. 1). The sample undergoes the first FMT during quenching and consequently was not recorded. The characteristic transformation temperatures, determined from the transformation cycle after heating up to 473 K, are martensite start, $M_s = 394$ K, and martensite finish, $M_f = 341$ K, for the FMT and austenite start, $A_s = 370$ K, and austenite finish, $A_f = 420$ K, for the RMT. Focusing on the heating curves, the heating up to 473 K modifies the characteristics of the reverse transformation. The second RMT has a slightly lower RMT interval, $A_f - A_s$, than the first RMT, with a higher $A_s$ and lower $A_f$. The transformation enthalpy for the first and second RMT are $\Delta H_{1st}^{m \rightarrow \beta} = 390$ J/mol and $\Delta H_{2nd}^{m \rightarrow \beta} = 460$ J/mol. Thus, the measured enthalpy and the peak temperature both increase after heating to 473 K. On the other hand, a value of $\Delta H_{2nd}^{\beta \rightarrow m} = 450$ J/mol for the second FMT has been obtained. The measured enthalpy agrees with the values reported for Cu-Al-Ni alloys transforming from $\beta$ to $\beta'$ martensite.[13,23]

The fraction of martensite as a function of temperature during the reverse MT has been estimated from the ratio of the integrated peak areas of the martensite and the $\beta$ phase of the ND spectra measured on heating at 10 K/$min^{-1}$. The inset in Fig. 1 shows the evolution of the martensite volume fraction during the first RMT (as-quenched) and for the second RMT (cycled). ND results agree with the calorimetric measurement. It must be pointed out that the martensite phase is absent at temperatures higher than 430 K, even during the first RMT where stabilization of the martensite phase could be expected.

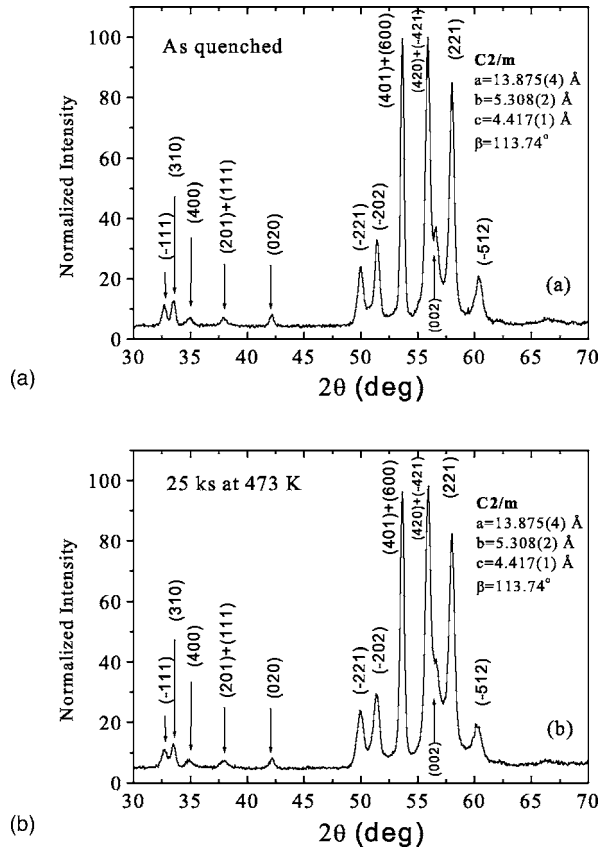


FIG. 2. (a) Room temperature neutron powder diffraction patterns measured in the as-quenched state (a) and after aging the alloy at 473 K for 25 ks (b).

The nature of the induced martensite has been determined by ND measurements at room temperature. Figures 2(a) and 2(b) show the neutron powder diffraction patterns measured in the as-quenched state, and after aging the alloy at 473 K during 25 ks, respectively. The indexing was performed according to a $C/2m$ monoclinic crystal structure (martensite $\beta'$ 18R) with $a=13.875$ Å, $b=5.308$ Å, $c=4.417$ Å, and $\beta=113.74°$. Comparing both patterns, it can be concluded that the aging at 473 K neither changes the kind of martensite formed nor the atomic order of the martensitic crystallographic structure. According to the diffusionless nature of the MT, the degree of order of the $\beta$ phase is inherited by the martensite. The $\beta$ phase observed above $A_s$ by ND always shows a $L2_1$ structure with the same degree of order. Thus, the differences in the RMT, shown in Fig. 1, cannot be attributed to any change in the crystallographic structure of the martensitic phase.

In the RUS technique, the elastic constants are determined from the fitting of the experimental resonance frequencies to the theoretical spectrum of the sample. The experimental resonances, the theoretical values obtained after refinement, and the error for the sample in $\beta$ phase state at 423 K are shown in Table I. A RUS eigenmode may depend on several elastic constants and their associated eigenfrequencies $f_n=f_n(C_{11},C_{44})$ have different sensitivities to $C_{ij}$ (isotropic crystals).[21] In order to see the influence of the different elastic constants on a particular vibration mode, Table I also shows the different theoretical sensitivities of the resonance frequencies, $A=(2C_{11}/f_n)(\partial f_n/\partial C_{11})$ and $B=(2C_{44}/f_n)\times(\partial f_n/\partial C_{44})$, corresponding to the measured vibration modes at 423 K. The $B$ value is much higher than $A$ for all the resonance frequencies, which means that the vibrational behavior in the studied frequency range is mainly controlled by the $C_{44}$ polycrystalline elastic constant. The refined $C_{11}$ and $C_{44}$ elastic constants allow one to determine the values of the Young modulus $E$ and shear modulus $G$ using

$$E=C_{44}\frac{3C_{11}-4C_{44}}{C_{11}-C_{44}} \text{ and } \quad G=C_{44}. \tag{2}$$

The deduced elastic constants of the $\beta$ phase from the spectrum at 423 K are $E^{\beta}=101\pm2$ GPa and $G^{\beta}=36.98\pm0.05$ GPa. These values are in good agreement with isotropic elastic constants obtained by averaging the single crystals values at room temperature for these alloys using the Hill approximation: $E^{\beta}=110$ GPa and $G^{\beta}=41$ GPa from Ref. 8, and $E^{\beta}=106$ GPa and $G^{\beta}=39$ GPa from Ref. 7. The slightly lower values of the present work are justified taking into account the higher measuring temperature. In order to connect elastic and thermal properties, the Debye temperature $\theta_D$ of the $\beta$ phase has been estimated using[24]

$$\theta_D=\left(6\pi^2\frac{N}{V}\right)^{1/3}\frac{\hbar}{k_B}v_o, \tag{3}$$

where $N/V$ is taken as the number of atoms per unit volume, $k_B$ is the Boltzmann's constant and the average sound velocity ($\nu_o$) is given by

$$\frac{1}{v_0^3}=\frac{1}{3}\left(\frac{1}{v_l^3}+\frac{2}{v_t^3}\right), \tag{4}$$

where the longitudinal and transverse sound velocities are $v_l=\sqrt{C_{11}/\rho}$ and $v_t=\sqrt{C_{44}/\rho}$, respectively, $\rho$ being the density. Thus, the estimated Debye temperature for the $\beta$ phase is $\theta_D=325\pm3$ K. This value is 5% higher than the value estimated for a Cu-Al-Ni alloy with the present composition.[25]

The evolution of $E$ and $G$ during the first RMT and the subsequent FMT is shown in Figs. 3(a) and 3(b). Also shown in Fig. 3(b) is the internal friction determined from the width at half height of the resonance peak corresponding to a frequency of $f=986$ kHz. These two figures show remarkable features. The behavior of the moduli is discussed first. On heating both $E$ and $G$ are essentially constant between 300 K and 380 K. Both moduli increase on entering the $\beta$ phase. Cooling shows hysteresis, as expected, the transition back to the martensite occurring at a lower temperature, in agreement with the DSC measurements. Both moduli, on cooling, show a dip below the heating curves. The behavior of the internal friction is even more unusual. No internal friction peak is observed on heating; the loss shows only a slight decrease on entering the $\beta$ phase. On cooling the internal friction shows a peak at the temperature of the dips in the moduli. These same features have been observed in all the resonances, namely dips in the moduli and an internal friction peak on cooling, but the absence of these effects on heating. The effects observed on cooling (internal friction peak and moduli dips) are a general response for this kind of

TABLE I. Experimental resonant frequencies, theoretical values obtained after refinement, and the error corresponding to the measurement at 423 K ($C_{11}=174.45$ GPa and $C_{44}=36.98$ GPa). The theoretical sensitivities, $A=(2C_{11}/f_n)(\partial f_n/\partial C_{11})$ and $B=(2C_{44}/f_n)(\partial f_n/\partial C_{44})$, of the different resonances are also shown.

| Frequency (MHz) (Experimental) | Frequency (MHz) (Theoretical) | Error % | $A=\frac{2c_{11}}{f}\frac{\partial f}{\partial c_{11}}$ | $B=\frac{2c_{44}}{f}\frac{\partial f}{\partial c_{44}}$ |
|---|---|---|---|---|
| 0.403291 | 0.402785 | −0.13 | 0.000 | 1.000 |
| 0.492283 | 0.492327 | 0.01 | 0.088 | 0.912 |
| 0.521583 | 0.523328 | 0.33 | 0.089 | 0.911 |
| 0.703851 | 0.704707 | 0.12 | 0.056 | 0.944 |
| 0.714977 | 0.714001 | −0.14 | 0.017 | 0.983 |
| 0.763488 | 0.762599 | −0.12 | 0.023 | 0.977 |
| 0.783433 | 0.784844 | 0.18 | 0.014 | 0.986 |
| 0.794079 | 0.791596 | −0.31 | 0.002 | 0.998 |
| 0.896601 | 0.897739 | 0.13 | 0.024 | 0.976 |
| 0.943263 | 0.940971 | −0.24 | 0.111 | 0.889 |
| 0.959089 | 0.957159 | −0.20 | 0.027 | 0.973 |
| 0.971534 | 0.968835 | −0.28 | 0.030 | 0.970 |
| 0.986479 | 0.984102 | −0.24 | 0.030 | 0.970 |
| 0.998255 | 0.997574 | −0.07 | 0.062 | 0.938 |
| 1.047008 | 1.048238 | 0.12 | 0.012 | 0.988 |
| 1.071842 | 1.072384 | 0.05 | 0.013 | 0.987 |
| 1.081364 | 1.083670 | 0.21 | 0.020 | 0.980 |
| 1.102989 | 1.103090 | 0.01 | 0.006 | 0.994 |
| 1.130500 | 1.129512 | −0.09 | 0.047 | 0.953 |
| 1.139121 | 1.140995 | 0.16 | 0.068 | 0.932 |
| 1.149648 | 1.150071 | 0.04 | 0.079 | 0.921 |
| 1.194582 | 1.193652 | −0.08 | 0.074 | 0.926 |
| 1.205517 | 1.210126 | 0.38 | 0.004 | 0.996 |
| 0.000000 | 1.210853 | 0.00 | 0.007 | 0.993 |
| 1.214654 | 1.214989 | 0.03 | 0.144 | 0.856 |
| 1.218767 | 1.218527 | −0.02 | 0.093 | 0.907 |

transformation independent of the conditions of the measurements, i.e., isothermal or nonisothermal, and the range of frequencies, from Hz to MHz,[26,27] and are normally observed on heating and cooling. Furthermore, the lack of the internal friction peak at the dips in the moduli on heating have been checked also during the second RMT after heating the sample up to 473 K.

In order to study further the anomalous behavior detected in the elastic and calorimetric measurements during the first RMT, intermediate thermal treatments at 398 K, 403 K, and 408 K were performed on the as-quenched alloy. For DSC measurements the procedure was the following: the sample was heated on the DSC from room temperature to a temperature between $A_s$ and $A_f$ (into the retransformation range) and subsequently cooled to room temperature. Immediately a cycle of DSC measurements composed of a heating run up to 473 K (first RMT), followed by cooling to 250 K (second FMT), and then heating to 473 K (second RMT). The idea is to measure the MT on a sample that had previously suffered a partial martensite-austenite retransformation. During the heating to the intermediate temperature, a part of the martensite is retransformed to austenite (partial RMT). Then, after cooling to RT, there are two different martensitic regions: those formed directly after quenching and which have not transformed to austenite in the intermediate temperature treatment (unreversed martensite) and those regions that have previously retransformed in the intermediate temperature treatment (reversed martensite). Figure 4 shows the DSC thermograms obtained during the first RMT (dotted line) carried out on samples previously treated at 403 K. A double contribution is observed in the endothermic process with a sharp peak in the high-temperature side of the thermogram. This behavior agrees with the presence of two kinds of martensitic regions, reversed and unreversed. Figure 4 also shows the DSC corresponding to the MT cycle after heating up to 473 K (continuous lines). Both peaks, the exothermic one for the second FMT and the endothermic one for the second RMT, have again a double contribution, but the second RMT shows the sharp peak in the low-temperature side. As can be seen by comparing Figs. 1 and 4, the second RMT measured after a direct heating from room temperature to 473 K (Fig. 1) is different from a step heating to 473 K (Fig.

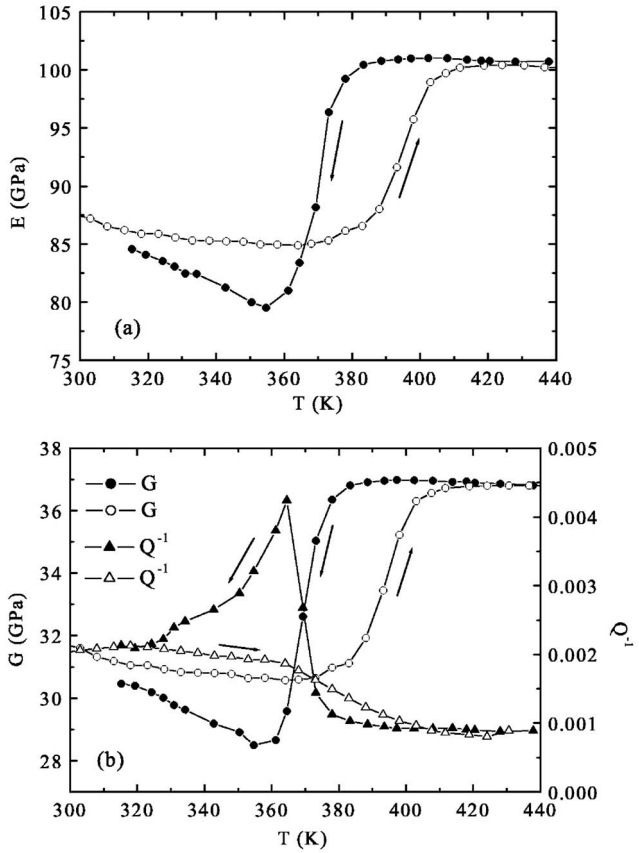


FIG. 3. Young modulus ($E$) (a) and shear modulus ($G$) and internal friction $Q^{-1}$ (b) during the first RMT (heating) and the subsequent FMT (cooling).

4). In this last case, the induced MT after heating to 473 K has a memory of the previous partial retransformation. The same behavior has been detected for the two other intermediate thermal treatments at 398 K and 408 K. Nevertheless,

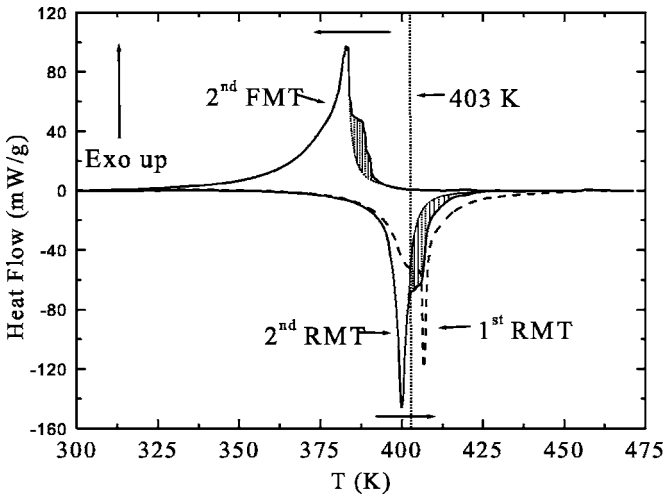


FIG. 4. DSC up to 473 K during the first RMT (dotted line) carried out on a sample preheated at 403 K. The full line shows the following cooling-heating run between 473 K and 250 K (second FMT and second RMT, respectively).

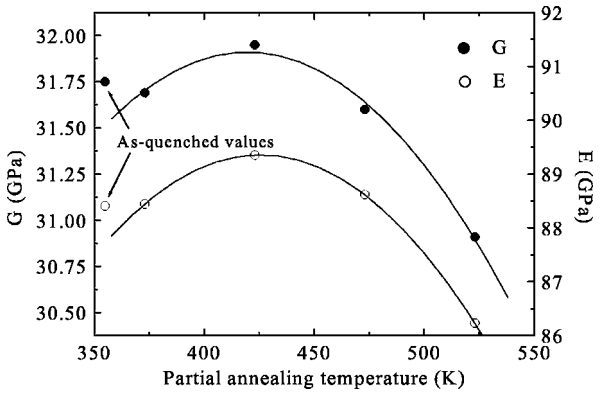


FIG. 5. Young modulus ($E$) and shear modulus ($G$) measured at room temperature as a function of the preheated intermediate temperature. The as quenched values are also shown.

partial retransformation on high-temperature recovered samples (above 500 K) does not show any double contribution.

In addition, $E$ and $G$ have been measured at room temperature, in the martensite phase, for samples previously retransformed by heating up to different intermediate temperatures, Fig. 5. For each measurement the sample was annealed at 1173 K during 1.8 ks, quenched in ice water, and subsequently thermally treated at the intermediate temperatures. Both elastic constants increase for intermediate heating below $A_f$, the end of the RMT, but higher intermediate temperatures induce a decrease of $E$ and $G$.

## IV. DISCUSSION

During a thermoelastic MT, a local energy equilibrium between chemical and nonchemical terms is established in the transforming region. Thus, there is a Gibbs free-energy balance between the difference in chemical Gibbs free energy for the $\beta$ and martensite phases, the stored elastic energy, and the energy dissipated by the frictional forces. The transformation hysteresis is controlled by the dissipative forces and the transformation range is controlled by both nonchemical terms. A necessary condition for a thermoelastic MT is the high mobility of boundary interfaces.

The internal friction spectrum obtained during a MT can be decomposed into three different contributions,[26]

$$IF(T) = IF_{Tr}(T) + IF_{PF}(T) + IF_{Int}(T). \quad (5)$$

$IF_{Tr}(T)$ is the transitory contribution that appears only during heating or cooling runs and it is related to the volume fraction $n$ of transformed phase per unit time, i.e., the displacement of interface boundaries over large distances, $IF_{Tr}(T) \propto \partial n / \partial T$.[26] Thus, this term becomes zero for isothermal RUS measurements. The $IF_{PF}(T)$ term is associated with the phase transformation itself and it responsible for the IF peak during isothermal measurements. It is related to an oscillating displacement of the interfaces between the $\beta$ phase and the martensite around their local thermoelastic equilibrium position in response to an oscillating applied stress.[28] The maximum value of $IF_{PF}(T)$, the IF peak, occurs at the

maximum area of interfaces, at around 50% of transformation.[29] In the case of IF measurements in the range of the Hz, a model was proposed for the $IF_{PF}(T)$ due to the $\beta/\beta'$ interface motion, which considers a microscopic stress hysteresis $\Delta\tau_m$ related to a shear deformation in the habit plane between both phases.[30] The value of $\Delta\tau_m$ depends strongly on the microstructure, i.e., the presence of precipitates in the matrix. The intrinsic term, $IF_{Int}(T)$, gives the IF contribution of each phase related to each own microstructure. Usually higher values of the $IF_{Int}(T)$ are measured in the martensite than in the $\beta$ phase due to the presence of the martensite domain interfaces.[26] During the MT the $IF_{Int}(T)$ is weighted by the volume fraction of each phase. In the RUS measurements, the last two contributions should be present in both the forward and the reverse MTs. In all the IF spectra measured during the first RMT, i.e., Fig. 3(b), the $IF_{PF}(T)$ peak is absent and only the change of the $IF_{Int}(T)$ from the $\beta$ phase values to a higher $IF_{Int}(T)$ level in the martensite phase is observed. On the contrary, the spectra carried out on cooling, Fig. 3(b), show both contributions, the $IF_{PF}(T)$ peak and the $IF_{Int}(T)$ background.

The results can be explained by taking into account the role of defects in the MT. The different mobility of defects in the two phases, and the concurrent recovery processes and MT in the same temperature range, are the origin of the observed behavior. For Cu-Al-Ni the vacancies are mobile in the $\beta$ phase above 373 K (Ref. 31) and the equilibrium vacancy concentration is achieved at about 530 K.[31,32] For instance, in a Cu-Al-Ni alloy with reverse MT temperatures $A_s=396$ K and $A_f=428$ K, the annealing of quenched vacancies occurs simultaneously with the appearance of the $\beta$ phase during the reverse MT.[32] (See below for more experimental support). Besides, in Cu-based SMA the vacancy migration energy in the martensite is higher than in the $\beta$ phase.[33] On the other side, vacancies in the temperature range of the reverse MT, 390 K to approximately 430 K, phase have enough mobility to migrate to interfaces, reducing the free energy of the structure, and pinning the martensite-austenite interfaces. The high density of quenched-in defects inherited by the martensitic phase during quenching produces a pinning of the interfaces, reducing their mobility and consequently promoting the lack of the $IF_{PF}(T)$ peak. The necessary high mobility of the interface boundaries is lost and the thermoelastic character of the MT is reduced. The disappearance of the dip of the dynamic moduli, $E$ and $G$, during the first RMT, Figs. 3(a) and 3(b), is due to the locking of the interfaces by the quenched-in defects, which promotes an increase of the dynamic moduli. (The moduli would be lower if the interfaces could move in response to the oscillating stress.) The result is the lack of the IF peak and the lack of the minimum in the elastic moduli in the first reverse MT. A similar absence of a dip in Young's modulus during the first RMT in Cu-Zn-Al alloys was observed by dynamic mechanical analysis (DMA) measurements.[34] Comparing this result with the present work there are some differences. The work performed in Ref. 34 is related to the strong stabilization that occurs on Cu-Zn-Al alloys ($M_s$ is $\approx$30 K higher for the first RMT than for the second RMT). The internal friction is measured at a constant heating rate in the range of the Hz, then they measured together the $IF_{Int}(T)$, $IF_{Tr}(T)$, and $IF_{PF}(T)$ terms. In that paper it is suggested that the poor mobility of the interfaces is responsible for the small decrease in the internal friction values as a consequence of a pinning mechanism operative in stabilized martensite. In our case, the difference in the transformation temperature between both RMTs is negligible, even the temperature is lower for the first RMT (Fig. 1). Besides, samples quenched or quenched and aged during 1 year at 300 K both show practically the same behavior. Thus, a static stabilization process due to isothermal aging in martensite state must be dismissed as the origin of the locking of the interfaces. On the other hand, studies performed on the same alloy shows an internal friction peak during heating and cooling at frequencies of around 1 Hz.[26] Both the $IF_{Tr}(T)$ and $IF_{PF}(T)$ terms are analyzed. During the RMT in that paper, the $IF_{PF}(T)$ peak is clearly observed at frequencies of 1 Hz. The lack of the internal friction peak and moduli dips during the RMT is only observed in the kHz range measurements. Then, different mechanisms must be involved in both frequency ranges as proposed by Stoiber *et al.*[30] In the high-frequency range, the IF could be associated to damping mechanism related to the mobility of the dislocations[30] which form the interface.[35,36]

After heating up to 473 K, the excess of quenched defects is not completely annealed, but the peak of IF, the $IF_{PF}(T)$ term, and the minimum in both elastic moduli are present during the FMT since the temperature range of transformation, 320–390 K, is lower than in the RMT and at these temperatures the migration of defects to interfaces is not allowed by their low mobility and the interface movement is observed. The main point is the existence of both the austenite-martensite interface and the mobility of defects in a particular temperature range. As Fig. 3(b) summarizes, the main difference between the MT on cooling and heating is the mechanical pinning of interfaces during the first reverse MT.

It was pointed out in the previous section that during a second RMT after heating up to 473 K, the IF peak and the minima in both moduli are all absent. An excess of vacancies remains in the $\beta$ phase after heating up to 473 K by taking into account that 530 K is required to completely anneal the excess of quenched vacancies.[31,32] Because of the low-oscillation amplitude of the ultrasonic waves generated in the sample during RUS measurements, the remaining concentration of quenched defects is enough to pin again the interfaces during the second RMT.

In a sample partially retransformed, as shown in Fig. 4, two kinds of martensitic regions are present: reversed and unreversed. In the reversed region the annealing of the excess of quenched defects starts in the $\beta$ phase due to their higher mobility in this phase. On the contrary, in the unreversed martensite region, the pinning of interfaces is enhanced by the partial heating. The result is a stabilization of the martensite in this region during the reverse transformation and the appearance of a sharp peak in the high-temperature side of the DSC, represented by the dotted line in Fig. 4. The mobility of the interfaces is so low that an overheating, an increase of $\Delta G_c$, is necessary to overcome the pinning force and to induce their movement during the

RMT, resulting in the sharp peak on the high-temperature side. Since the burst character of the transformation is enhanced (as evidenced by the sharp peak), the generation of defects is promoted. Defects, such as dislocations, play an important role in martensite nucleation since unstable zones are present around defects where the elastic constant $C'$ softens dramatically.[14] According to the first-order character of the MT, an incomplete softening of $C'$, sensitive to $\{011\}\times\langle 0\bar{1}1\rangle$ shear strains, has been measured when the temperature approaches $M_s$. Localized soft modes models for the MT have been proposed considering the effect of defects on the stability of the $\beta$ phase.[4] Thus, after the first RMT, above $A_s$, the $\beta$ phase has two regions with different concentrations of defects corresponding to the two kinds of martensitic regions, reversed and unreversed, the defect concentration being higher for the $\beta$ phase coming from the unreversed martensite region. Since the martensite nucleation is enhanced by the presence of defects, two steps appear during the next MT cycle, shown by continuous lines in Fig. 4. The shadow areas in the DSC thermograms for the second FMT and second RMT correspond to the $\beta$-phase region with higher defect concentration.

The evolution of elastic constants measured at room temperature, in the martensite, as a function of the highest temperature achieved previously (Fig. 5) agrees with this assumption. Heating up to temperatures in the range of the reverse MT promotes the pinning of interfaces and consequently higher values of $E$ and $G$ are measured at room temperature. On the contrary, for heating up above $A_s$, in the $\beta$ phase region, the values of both moduli diminish, which is attributed to fewer pinning defects. The lowest values correspond to 523 K where the equilibrium concentration of vacancies is achieved in the $\beta$ phase.

Another DSC measurement was carried out to study the role of vacancy concentration and defect distribution on the MT. The sample was heated up to 473 K to anneal the excess of defects, cooled to the martensite, partially retransformed up to 403 K, cooled to room temperature (that is, partially retransformed after the second FMT) and finally the RMT was recorded. Figure 6 shows this measurement and the one corresponding to a sample heated up to 403 K from the as quenched state, as shown in Fig. 4 (dotted line). The double-contribution effect is much less for the sample heated up to 473 K, but even in this case the pinning of interfaces by defects during the partial retransformation modifies the local thermoelastic equilibrium of the MT inducing the stabilization of martensite as can be deduced from the small sharp peak in the thermogram (solid line). In addition, this result confirms the locking of interfaces during the second RMT.

The results have been explained taking into account the role of defects in the MT and the concurrent recovery processes and MT in the same temperature range. In order to corroborate the proposed assumption, another Cu-Al-Ni SMA with a slightly different composition, $Cu_{69}Al_{27.4}Ni_{3.6}$, undergoing the MT at low temperature, $M_s \approx 173$ K,[37] has been used, which allows one to isolate the vacancy annealing processes. The inset in Fig. 6 shows the exothermic process linked to the annealing of quenched-in vacancies during heating in this alloy. The vacancies recovery in both alloys

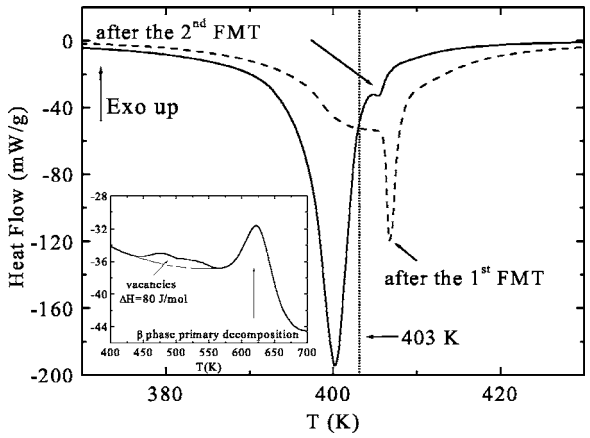


FIG. 6. DSC measurements carried out during the RMT on two samples partially retransformed up to 403 K: after the second FMT (full line) and after the first FMT, that is, as-quenched state (dotted line, which corresponds to the sample shown in Fig. 4). The inset shows the DSC measurement, heating rate 4 K min$^{-1}$, in a $Cu_{69}Al_{27.4}Ni_{3.6}$ alloy with $M_s \approx 173$ K. The first exothermic peak corresponds to the annealing of excess of quenched-in vacancies.

occurs in austenite phase then, it must proceed is a similar way. The DSC shown in this inset is performed at a constant heating rate of 4 K min$^{-1}$, whereas the RUS measurements are carried out at constant temperature and accumulative effects must be taken into account. The idea of high mobility of vacancies in the 390–430 K temperature range and low mobility between 320 K and 390 K seem to agree with the temperature range where the recovery of vacancies occurs as shown in the inset of Fig. 6. At a heating rate of 4 K min$^{-1}$ the exothermic process appears above 430 K. This indicates that the recovery of vacancies at constant temperature must take place in relatively short times in the 390–430 K temperature range just below the appearance of the exothermic process. On the other side, at lower temperatures (in the 320–390 K range), the recovery needs much longer time.

Finally, the difference of transformation enthalpy measured between the first and the second RMT, $\Delta H_{1st}^{m\to\beta} = 390$ J/mol and $\Delta H_{2nd}^{m\to\beta} = 460$J/mol, Fig. 1, can be explained by taking into account the heat released during the annealing of quenched vacancies. The concentration of vacancies retained at room temperature during quench from 1173 K to 273 K has been estimated as $C_v \approx 10^{-3}$, taking the values of $E_f = 0.54$ eV,[31] and $E_m = 0.63$ eV,[38] for the formation and migration energy of vacancies in Cu-Al-Ni, a quenching rate of $\dot{T} = 2000$ K/s,[38,39] and integrating the differential equation that satisfies the vacancy concentration during a quench at a constant quenching rate.[40] The calculated value of the enthalpy of the exothermic process related to the annealing of this excess of quenched vacancies is $\Delta H \approx 50$ J/mol. To check experimentally the validity of this estimation, we have calculated the area of the exothermic peak linked to the annealing of the quenched-in vacancies for the low-temperature MT alloy, shown in the inset in Fig. 6. The obtained value is $\Delta H = 80 \pm 10$ J/mol. Although the quenching process could produce different results when the quench is to martensite or to austenite, the measured value can be considered as an estimation of the enthalpy associated

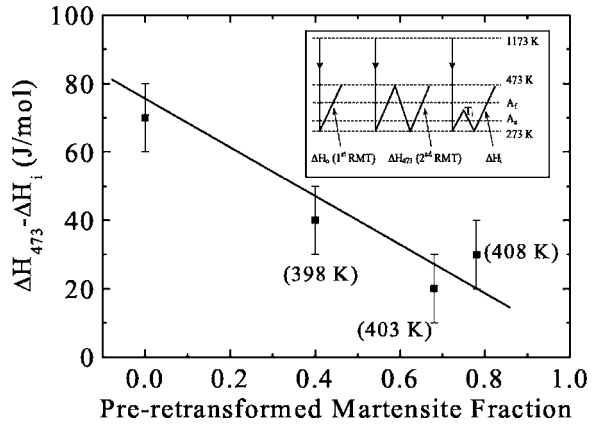


FIG. 7. Difference between the enthalpy measured during the RMT in a sample previously heated up to 473 K (after the second FMT), $\Delta H_{473}$, and the enthalpy of the first RMT, $\Delta H_i$, for samples previously heated up to different temperatures ($T_i$=398 K, 403 K, and 408 K), as a function of the preretransformed martensite fractions. The first point corresponds to the difference $\Delta H_{473}-\Delta H_0$ where $\Delta H_0$ is the enthalpy of the first RMT for the as quenched sample (zero fraction of preretransformed martensite). The inset shows the thermal treatments performed on the samples. The vertical lines correspond to the quenching process from 1273 K to ice water. The enthalpies ($\Delta H_0$, $\Delta H_{473}$ and $\Delta H_i$) were measured during the last heating at the end of the corresponding treatments (indicated by arrows). $T_i$ is an intermediate temperature between $A_s$ and $A_f$ and is also shown in Fig. 7 (in parentheses).

with the vacancies recovery. The movement of vacancies as described in the text agrees with the temperature range of this exothermic process. In both alloys the vacancies recovery is taking place in the austenite phase and the diffusion process must be similar. Thus, these two values for the vacancy annealing contribution, 50 J/mol estimated and 80 J/mol measured, are in good agreement with the 70 J/mol difference from Fig. 1. The vacancy annealing process was studied further as a function of the partial annealing temperature.

Since the recovery of defects occurs simultaneously with the MT, it is expected that an intermediate treatment above $A_s$ reduces the remaining density of defects in the sample. For a 473 K treated sample (above $A_f$), the full sample transforms to $\beta$ phase. Although the equilibrium concentration is not achieved at 473 K, this partial treatment allows one to take its achieved defect density as a reference to see the effect of lower intermediate temperatures. In any case, the higher the intermediate temperature, the lower the remaining density of defects after cooling to martensite. Figure 7 shows the difference between the enthalpy measured during the RMT in a sample previously heated up to 473 K (second RMT), $\Delta H_{473}$, and the enthalpy, $\Delta H_i$, for samples previously heated up to different intermediate temperatures ($T_i$=398 K, 403 K, and 408 K) corresponding to different preretransformed martensite fractions that were estimated from ND results (inset in Fig. 1). To clarify the analysis, the inset in Fig. 7 shows the different thermal treatment performed on the samples. The leftmost point in Fig. 7 corresponds to the difference $\Delta H_{473}-\Delta H_0$ where $\Delta H_0$ is the enthalpy of the first RMT without previous heating (as quenched state), that is, at zero fraction of preretransformed martensite. As mentioned above, $\Delta H_{473}-H_0=70\pm10$ J/mol is in good agreement with both the estimated and measured values of the heat released during the annealing of this excess of quenching vacancies. Therefore, the difference of enthalpies between the first RMT and the second RMT is linked to the exothermic process of vacancy annealing. In addition, the higher the temperature previously achieved (or the preretransformed martensite fraction), the lower the difference $\Delta H_{473}-\Delta H_i$ according to the lower remaining concentration of quenching defects.

## V. CONCLUSIONS

The role of defects on a first-order transformation has been analyzed in the present work. The influence of defects on the mobility of $\beta$-martensite interfaces has been studied in a Cu-Al-Ni shape-memory alloy undergoing a martensitic transformation in the same temperature range where the recovery of defects takes place. An anomalous behavior has been observed mainly by RUS since the IF peak that is present during cooling completely disappears on heating. The high density of defects has enough mobility to migrate to the $\beta$-martensite interface during the reverse martensitic transformation and produce a pinning effect. This effect is also demonstrated by calorimetric results and, in fact, shows a secondary memory effect in samples that have been previously partially retransformed. On the other side, the mobility of defects during cooling is not high enough in the lower temperature range corresponding to the forward transformation, and the interfaces are nearly free, leading to a large value of the internal friction and its associated reduced elastic constants. The different mobility of defects in the two phases, and the concurrent existence of both the recovery processes and the martensitic transformation in the same temperature range, are the origin of the observed behavior. Stabilization takes place when vacancies are mobile and this occurs when the MT proceeds. This effect shows the outstanding role of defects on the thermoelastic equilibrium during a first-order structural transition. The proposed mechanism is general, and may apply to other transitions than the one reported in this paper

## ACKNOWLEDGMENTS

This work has been carried out with the financial support of the Spanish Ministerio de Ciencia y Tecnología (Projects No. MAT2000-1676-C02-02 and No. MAT2003-05243). The Institut Laue-Langevin, D20 and D1A installations (Grenoble, France) is acknowledged for the allocated neutron beamtime (5-25-73 and 5-24-146). The authors wish to thank Professors. J. San Juan and M.L. Nó for supplying the alloy.

*Corresponding author. Email address: ipzlanda@unavarra.es

[1] L. Delaey, in *Materials Science and Technology*, edited by P. Haasen (VCH, Weinheim, 1991), Vol. 5, p. 339.
[2] M. Cohen, G. B. Olson and P. C. Clapp, *Proceedings of the ICOMAT'79, MIT, Cambridge, MA* (MIT Press, Boston, 1980), p. 1.
[3] C. Zener, Phys. Rev. **71**, 846 (1947).
[4] A. Planes, and Ll. Mañosa, Solid State Phys. **55**, 159 (2001).
[5] G. Guenin, M. Morin, P. F. Gobin, W. Dejonghe, and L. Delaey, Scr. Metall. **11**, 1071 (1977).
[6] A. Planes, Ll. Mañosa, D. Rios-Jara, and J. Ortin, Phys. Rev. B **45**, 7633 (1992).
[7] Ll. Mañosa, M. Jurado, A. Planes, J. Zarestky, T. Lograsso, and C. Stassis, Phys. Rev. B **49**, 9969 (1994).
[8] V. Recarte, J. I. Pérez-Landazábal, M. L. Nó, and J. San Juan, Mater. Sci. Eng., A **370**, 488 (2004).
[9] G. B. Olson and M. Cohen, Scr. Metall. **9**, 1247 (1977); **11**, 345 (1977).
[10] M. Grujicic and G. B. Olson, Interface Sci. **6**, 155 (1998).
[11] H. Warlimont and L. Delaey, Prog. Mater. Sci. **18**, 1 (1974).
[12] J. Ortín and A. Planes, Acta Metall. **36**, 2417 (1988); **37**, 1433 (1989).
[13] V. Recarte, J. I. Pérez-Landazábal, P. P. Rodríguez, E. H. Bocanegra, M. L. Nó, and J. San Juan, Acta Mater. **52**, 3941 (2004).
[14] G. Guenin and P. F. Gobin, Metall. Trans. A **13A**, 1127 (1982).
[15] M. Grujicic, G. B. Olson, and W. S. Owen, Metall. Trans. A **16A**, 1713 (1985); **16A**, 1723 (1985); **16A**, 1735 (1985).
[16] S. Kustov, J. Pons, E. Cesari, and J. Van Humbeeck, Acta Mater. **52**, 3075 (2004).
[17] S. Kustov, J. Pons, E. Cesari, and J. Van Humbeeck, Acta Mater. **52**, 4547 (2004).
[18] S. Kustov, J. Pons, E. Cesari, and J. Van Humbeeck, Acta Mater. **52**, 3083 (2004).
[19] J. San Juan, R. B. Pérez-Sáez, V. Recarte, M. L. Nó, G. Caruana, M. Lieblich, and O. A. Ruano, J. Phys. IV **5**, 919 (1995).
[20] R. B. Pérez-Sáez, V. Recarte, M. L. Nó, O. A. Ruano, and J. San Juan, Adv. Eng. Mater. **2**, 49 (2000).
[21] A. Migliori and J. L. Sarrao, *Resonant Ultrasonic Spectroscopy* (John Wiley & Sons, New York, 1997).
[22] R. G. Leisure and F. A. Willis, J. Phys.: Condens. Matter **9**, 6001 (1997).
[23] C. Picornell, J. Pons, and E. Cesari, Acta Mater. **49**, 4221 (2001).
[24] G. Grimvall, *Thermophysical Properties of Materials* (Elsevier, North Holland, Amsterdam, 1999).
[25] R. Romero and J. L. Pelegrina, Mater. Sci. Eng., A **354**, 243 (2003).
[26] R. B. Pérez-Sáez, V. Recarte, M. L. Nó, and J. San Juan, Phys. Rev. B **57**, 5684 (1998).
[27] *Phase Transformations in Mechanical Spectroscopy Q-1 2001*, edited by R. Schaller, G. Fantozzi, and G. Gremaud (Trans Tech Publications, Enfield, 2001), chap. 5, p. 382.
[28] J. E. Bidaux, R. Schaller, and W. Benoit, Acta Metall. **37**, 803 (1989).
[29] J. X. Zhang, P. C. W. Fung, and W. G. Zeng, Phys. Rev. B **52**, 268 (1995).
[30] J. Stoiber, J. E. Bidaux, and R. Gotthardt, Acta Metall. Mater. **42**, 4059 (1994).
[31] H. Fukushima and M. Donaya, J. Phys. F: Met. Phys. **9**, L177 (1979).
[32] D. Segers, I. Hurtado, L. Dorikens-Vanpraet, and J. Van Humbeeck, Mater. Sci. Forum **175–178**, 513 (1995).
[33] D. Segers, J. Van Humbeeck, L. Dorikens-Vanpraet, I. Lemahieu, and M. Dorikens, Scr. Metall. **22**, 521 (1988).
[34] C. Seguí and E. Cesari, J. Phys. IV **5**, C8–835 (1995).
[35] R. C. Pond, S. Celotto, and J. P. Hirth, Acta Mater. **51**, 5385 (2003).
[36] R. C. Pond and X. Ma, Z. Metallkd. **96**, 1124 (2005).
[37] J. I. Pérez-Landazábal, V. Recarte, and V. Sánchez-Alarcos, J. Phys.: Condens. Matter **17**, 4223 (2005).
[38] V. Recarte, R. B. Pérez-Sáez, M. L. Nó, and J. San Juan, J. Appl. Phys. **86**, 5467 (1999).
[39] A. Planes, R. Romero, and Ahlers, Acta Metall. Mater. **38**, 757 (1990).
[40] A. Varschavsky and E. Donoso, Mater. Sci. Eng. A **212**, 265 (1996).